Applied Physics Letters

Terahertz field depolarization and absorption within composite media

Cite as: Appl. Phys. Lett. **115**, 041901 (2019); https://doi.org/10.1063/1.5101068
Submitted: 23 April 2019 . Accepted: 03 July 2019 . Published Online: 24 July 2019

Mark H. Bergen, Jason Reich, Tyler Ho, Flynn Clark, Matthew Reid, and Jonathan F. Holzman

Applied Physics Letters ARTICLE scitation.org/journal/apl

Terahertz field depolarization and absorption within composite media

Cite as: Appl. Phys. Lett. **115**, 041901 (2019); doi: 10.1063/1.5101068
Submitted: 23 April 2019 · Accepted: 3 July 2019 ·
Published Online: 24 July 2019

Mark H. Bergen,[1,a)] Jason Reich,[2] Tyler Ho,[1] Flynn Clark,[1] Matthew Reid,[2] and Jonathan F. Holzman[1]

AFFILIATIONS

[1]Faculty of Applied Science, The University of British Columbia, 1137 Alumni Avenue, Kelowna, British Columbia V1V 1V7, Canada
[2]Department of Physics, University of Northern British Columbia, 3333 University Way, Prince George, British Columbia V2N 4Z9, Canada

[a)]Author to whom correspondence should be addressed: mark.bergen@alumni.ubc.ca

ABSTRACT

In this work, we pursue a deeper understanding of the expression of the inclusion morphology and index contrast in the refraction and absorption characteristics of composites within the terahertz (THz) spectrum. The composites are composed of SiO_2 and Si nanoparticles as well as SiO_2 and Si microparticles functioning as deeply subwavelength inclusions in a polydimethylsiloxane (PDMS) host. Terahertz time-domain spectroscopy is used for experimental characterization of the composites over a wide range of volumetric fractions, and the trends that emerge are contrasted to theoretical predictions from the Bruggeman model. It is found that the refraction characteristics have a heightened dependence on the inclusions' shape when their index contrast with respect to the host becomes sufficiently large. We attribute such a correlation to terahertz field depolarization that occurs within inclusions at high index contrasts and the dependence of the fields to the inclusions' shape—as defined by a depolarization factor in the generalized form of the Bruggeman model. Moreover, it is found that the absorption characteristics have a heightened dependence on the inclusions' size when that size becomes sufficiently small. We attribute this to the manifold of surface states that form in small inclusions, due to their high surface-to-volume ratio, which raises the absorption beyond that of the bulk. It is concluded that the Bruggeman model can accurately characterize the refraction and absorption of THz radiation within composites having deeply subwavelength inclusions if their (shape-dependent) polarization and (size-dependent) absorption are suitably defined.

Terahertz (THz) radiation resides within a gap in the electromagnetic spectrum between the domains of radio frequency and infrared radiation. This unique position has enabled many applications, including THz imaging,[1] communications,[2,3] and spectroscopy.[4–6] These applications have relied upon the established refraction and absorption characteristics of conventional materials within the THz spectrum—although there is growing interest in tailoring such characteristics to specific applications. Composite materials emerged to meet this demand.[3,7–10]

Composites are composed of dielectric inclusions, such as nanoparticles or microparticles, within a host, typically a polymer. In these materials, the volumetric fraction of inclusions can be tailored to bring about specific refraction and absorption characteristics, and the physical form can be molded to the demands of the application. Nonetheless, it can be difficult to achieve the sought-after refraction and absorption characteristics for such composites due to the complex nature of the polarizability in the inclusions. A deeper understanding is warranted.

A variety of effective medium theories can be applied to understand the refraction and absorption characteristics of composites.[11–14] Such theories are founded upon models whose assumptions largely dictate the extent of their success. The Maxwell-Garnett model, as the simplest, assumes that the inclusions make up only a small volumetric fraction of the composite and that they are both spherical and much smaller than the wavelength of the incident radiation. Thus, the model is particularly effective in characterizing composites with low concentrations of small spherical inclusions.[11] The Bruggeman model extends the Maxwell-Garnett model by allowing for any volumetric fraction of inclusions. This lets the Bruggeman model characterize a wider array of composites,[9–12] although it still assumes that the inclusions are much smaller than the wavelength. In practice, it is found that the inclusion morphology, i.e., shape and size, together with the index contrast, i.e., ratio of inclusion-to-host refractive indices, can form a complex interplay that must be characterized and ultimately understood to realize an effective model. This is particularly true for THz radiation,[11] because it is often subject to large dielectric constants,

forcing one to consider inclusion morphology, and pronounced absorption, resulting from the manifold of surface states within inclusions.

In this paper, we pursue a deeper understanding of the expression of the inclusion morphology and index contrast in the refraction and absorption characteristics of composites within the THz spectrum. Terahertz time-domain spectroscopy (TDS) is used for experimental characterization of composites with polydimethylsiloxane (PDMS) as a host and an assortment of deeply subwavelength inclusions, being smaller than one-hundredth of the wavelength. The inclusions are composed of SiO_2 (with a low refractive index) and Si (with a high refractive index) in the form of nanoparticles (having a roughly spherical shape) and microparticles (having a highly irregular shape). The experimental characterization is carried out for a wide range of volumetric fractions, and the trends that emerge are contrasted to theoretical predictions of the Bruggeman model.

The Bruggeman model is a foundational effective medium theory for studies of composites within the THz spectrum[9–13] and is applied in this work. The model quantifies the refraction and absorption characteristics of a composite, with a volumetric fraction of V, via[13]

$$(1-V)\frac{\tilde{\varepsilon}_h(\omega)-\tilde{\varepsilon}(\omega)}{N\tilde{\varepsilon}_h(\omega)+(1-N)\tilde{\varepsilon}(\omega)}+V\frac{\tilde{\varepsilon}_i(\omega)-\tilde{\varepsilon}(\omega)}{N\tilde{\varepsilon}_i(\omega)+(1-N)\tilde{\varepsilon}(\omega)}=0, \quad (1)$$

where $\tilde{\varepsilon}_h(\omega)$, $\tilde{\varepsilon}_i(\omega)$, and $\tilde{\varepsilon}(\omega)$ are the complex dielectric constants of the host, inclusions, and overall composite, respectively, and ω is the angular frequency of the incident radiation. The depolarization factor, N, appears in this equation to generalize the Bruggeman model and its description of dielectric polarization to inclusions of arbitrary shape. It does so by characterizing the distribution of bound charges on the inclusions' surfaces and the depolarization field that such charges form in opposition to the applied electric field. For spherical inclusions, the depolarization factor is $N=1/3$.[9,12] For irregular inclusions at the same orientation, the depolarization factor depends upon orientation and takes on values between $N=0$ and $N=1$.[14,15] For irregular inclusions at random orientations, as seen in this work, a weighted average of the depolarization field from inclusions over all orientations is used to define an aggregate depolarization factor that takes on values between $N=0$ and $N=1/3$.[15] Ultimately, Eq. (1) is manipulated to give an explicit expression for $\tilde{\varepsilon}(\omega)$, which is used to determine the real valued refractive index, $n(\omega)$, and extinction coefficient, $\kappa(\omega)$, of the composite using $\sqrt{\tilde{\varepsilon}(\omega)}=n(\omega)-j\kappa(\omega)$. Through this generalized Bruggeman model, the depolarization factor, N, is treated as a fitting parameter that yields insight into the inclusions' shape. The complex dielectric constant of the inclusions, $\tilde{\varepsilon}_i(\omega)$, is modeled using the Drude model because the inclusions can, in general, exhibit free-carrier dispersion, with characteristics defined by the plasma frequency and scatter time.

Experimental characterization of refractive indices and extinction coefficients was carried out for a wide variety of composite samples using a THz TDS system. The system made use of a 780-nm pulsed laser (Toptica Photonics, FFS.SYS-2B), with a 100-fs pulse duration and a 90-MHz repetition rate, seeding a photoconductive THz emitter (Ekspla, EMT-08) with 25 mW of power and a photoconductive THz detector (Ekspla, DET-08) with 10 mW of power. This produced THz radiation spanning 0.2–1.5 THz. Measurements from this system were fed into a parameter extraction algorithm to obtain the refractive index, $n(\omega)$, and extinction coefficient, $\kappa(\omega)$.[13] The composite samples made use of PDMS (Sylgard 184) as a host, at a 20:1 base-to-curing-agent ratio, with nanoparticles and microparticles of SiO_2 and Si (US Research Nanomaterials) as the inclusions. Scanning electron microscopy (SEM) images of the nanoparticles and microparticles are shown in Fig. 1. The nanoparticles and microparticles are characterized by a mean plus/minus standard deviation of their size and shape, as defined by eccentricity $e=(1-(b/a)^2)^{1/2}$, where a and b are the lengths along the semimajor and semiminor axes, respectively. The SiO_2 nanoparticles, shown in Fig. 1(a), are 58 ± 11 nm in size and roughly spherical, with an eccentricity of 0.47 ± 0.26. The SiO_2 microparticles, shown in Fig. 1(b), are 4.3 ± 1.6 μm in size and highly irregular, with an eccentricity of 0.79 ± 0.18. The Si nanoparticles, shown in Fig. 1(c), are 36 ± 5.9 nm in size and roughly spherical, with an eccentricity of 0.49 ± 0.20. The Si microparticles, shown in Fig. 1(d), are 4.1 ± 3.2 μm in size and highly irregular, with an eccentricity of 0.79 ± 0.19. The SiO_2 and Si nanoparticles are roughly spherical due to their synthesis via thermal processes, allowing their surface energy to be minimized. The SiO_2 and Si microparticles are highly irregular due to their synthesis by mechanical disaggregation. The standard deviations in size of the SiO_2 and Si nanoparticles are dictated largely by the 5-nm measurement resolution of the SEM imaging, while the standard deviations in size for the SiO_2 and Si microparticles are dictated largely by their wide ranges in size. The larger standard deviations in eccentricity for the nanoparticles are due mainly to the increased sensitivity of eccentricity to axis lengths when the lengths are similar. The above nanoparticles and microparticles were used to fabricate samples with volumetric fractions of inclusions that spanned from zero up to the onset of agglomeration, being 7%, 40%, 5%, and 30%, respectively. (Agglomeration manifests itself as an inability to uniformly disperse the nanoparticles and microparticles throughout the host due to their high surface energy, and thus, it appears at lower

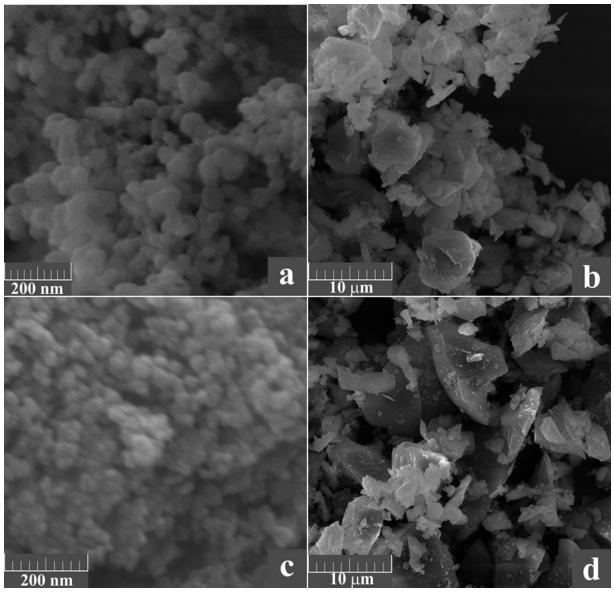

FIG. 1. Representative SEM images of the (a) SiO_2 nanoparticles, (b) SiO_2 microparticles, (c) Si nanoparticles, and (d) Si microparticles.

volumetric fractions for the nanoparticles in comparison to the microparticles[16]). Once mixed, the samples were degassed in a vacuum chamber for 30 min and then cured at room temperature for 48 h. Our prior work has shown that this process yields the lowest absorption in PDMS.[5] After curing, each sample was mounted as a free-standing slab for the measurement in the THz TDS system.

The refractive index and extinction coefficient are plotted for a set of representative samples as a function of frequency in Fig. 2. The results are shown for representative nano-SiO_2, micro-SiO_2, nano-Si, and micro-Si composites with volumetric fractions of 6.4%, 25.9%, 4.8%, and 20.3%, respectively. The frequency range of 500 GHz–1 THz was selected because it yields clear spectra for samples with all combinations of inclusion materials, sizes, and volumetric fractions. The trends for both the refractive index, Fig. 2(a), and the extinction coefficient, Fig. 2(b), are primarily constant over the displayed frequency range. The slight decrease in the refractive index with increasing frequency for all samples in Fig. 2(a) is attributed to the PDMS host,[6] while the slight decrease in the extinction coefficient of the micro-Si composite with increasing frequency in Fig. 2(b) is attributed to free-carrier dispersion (and will later be quantified via the Drude model).

The refraction and absorption characteristics for the composite samples are shown in Fig. 3 as a function of volumetric fraction. Here, the displayed data points denote mean values across the frequency range of 500 GHz–1 THz, and the displayed error bars show the standard deviations in the measurements arising from inaccuracies in sample thickness and homogeneity. Experimental results for the refractive index, $n(\omega)$, and extinction coefficient, $\kappa(\omega)$, are shown in Figs. 3(a) and 3(b) for the nano-SiO_2 composites (as open red circles) and micro-SiO_2 composites (as solid black circles), respectively. Experimental results for the refractive index, $n(\omega)$, and extinction coefficient, $\kappa(\omega)$, are shown in Figs. 3(c) and 3(d) for the nano-Si composites (as open red circles) and micro-Si composites (as solid black circles), respectively. Theoretical results from the Bruggeman model are displayed in all the figures for the nano-SiO_2 and nano-Si composites (as dotted red curves, for spherical inclusions, i.e., $N = 1/3$) and the micro-SiO_2 and micro-Si composites (as dashed black curves, for irregular inclusions, i.e., $N = 1/9$). The theoretical results were generated by solving Eq. (1) for the complex dielectric constant of the composite, $\tilde{\varepsilon}$, and computing its corresponding refractive index, $n(\omega)$, and extinction coefficient, $\kappa(\omega)$. The computations make use of fixed parameters for the refractive index of PDMS (1.56) and extinction coefficient of PDMS (0.044), having been obtained via independent measurements and confirmed with the literature.[6] The refractive indices and extinction coefficients of SiO_2 and Si are extracted as fitting parameters, as are the depolarization factors (with distinct fitting parameters used for the nanoparticles and microparticles).

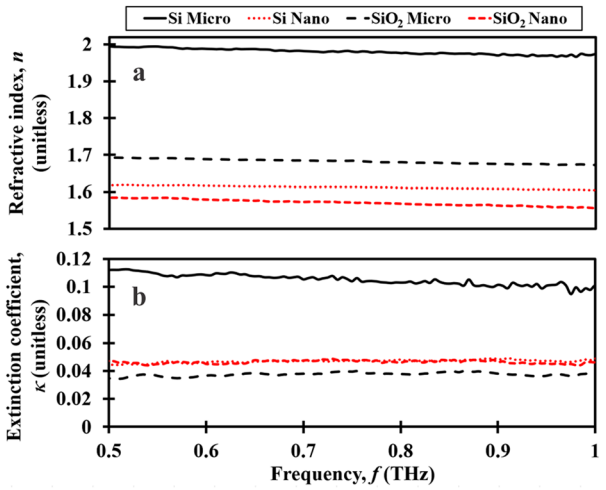

FIG. 2. Refraction and absorption characteristics of representative composites. The (a) refractive index and (b) extinction coefficient are shown for a nano-SiO_2 composite with a volumetric fraction of $V = 6.4\%$ (short dashed red line), a micro-SiO_2 composite with a volumetric fraction of $V = 25.9\%$ (long dashed black line), a nano-Si composite with a volumetric fraction of $V = 4.8\%$ (dotted red line), and a micro-Si composite with a volumetric fraction of $V = 20.3\%$ (solid black line).

Figure 3(a) shows theoretical and experimental results for the refractive index of the nano-SiO_2 and micro-SiO_2 composites. The experimental results show an increasing refractive index for the nano-SiO_2 composites, from 1.56 to 1.61 as the volumetric fraction rises to 7%, and an increasing refractive index for the micro-SiO_2 composites, from 1.56 to 1.75 as the volumetric fraction rises to 40%, suggesting that the refractive index of the SiO_2 is greater than that of PDMS. The theoretical results of the generalized Bruggeman model, obtained by curve-fitting Eq. (1) with the refractive index of SiO_2 and depolarization factors extracted as fitting parameters, show good agreement with these experimental results. The theory suggests that the refractive index of the SiO_2 is 2.04, which agrees with the literature for bulk SiO_2,[7] and that the depolarization factors of the SiO_2 nanoparticles and microparticles are $N = 1/3$ and $N = 1/9$, respectively. As previously discussed, the SiO_2 nanoparticles are roughly spherical explaining their depolarization factor of $N = 1/3$, and the SiO_2 microparticles are highly irregular explaining their reduced depolarization factor of $N = 1/9$. The results for the nano-SiO_2 and micro-SiO_2 composites show good agreement between the experiment, with respective standard deviations of 7.6×10^{-3} and 1.4×10^{-2}, and theory, with respective correlation coefficients of +0.86 and +0.98. Moreover, the results suggest that depolarization is of little consequence in composites having a low index contrast between the inclusions and host—as is the case for these SiO_2 nanoparticles and microparticles in PDMS.

Figure 3(b) shows theoretical and experimental results for the extinction coefficient of the nano-SiO_2 and micro-SiO_2 composites. The experimental results show an increasing extinction coefficient for the nano-SiO_2 composites, albeit slight, from 0.044 to 0.052 as the volumetric fraction rises to 7%, and a decreasing extinction coefficient for the micro-SiO_2 composites, from 0.044 to 0.024 as the volumetric fraction rises to 40%. The dissimilar trends suggest that the extinction coefficient of the SiO_2 nanoparticles is slightly greater than that of PDMS, while the extinction coefficient of the SiO_2 microparticles is far less than that of PDMS. Such a finding is corroborated by the theory. The theoretical results of the generalized Bruggeman model are obtained by curve-fitting Eq. (1) with the extinction coefficient of SiO_2 extracted as a fitting parameter and the depolarization factors of the nanoparticles and microparticles fixed at the aforementioned values of $N = 1/3$ and $N = 1/9$, respectively. The results for the micro-SiO_2 composites show good agreement between the experiment, with a standard deviation of 4.3×10^{-3}, and theory, at a correlation coefficient of +0.86. Moreover, the fitting yields an extinction coefficient of 2.8×10^{-4} for SiO_2, which agrees with the literature for bulk quartz.[4]

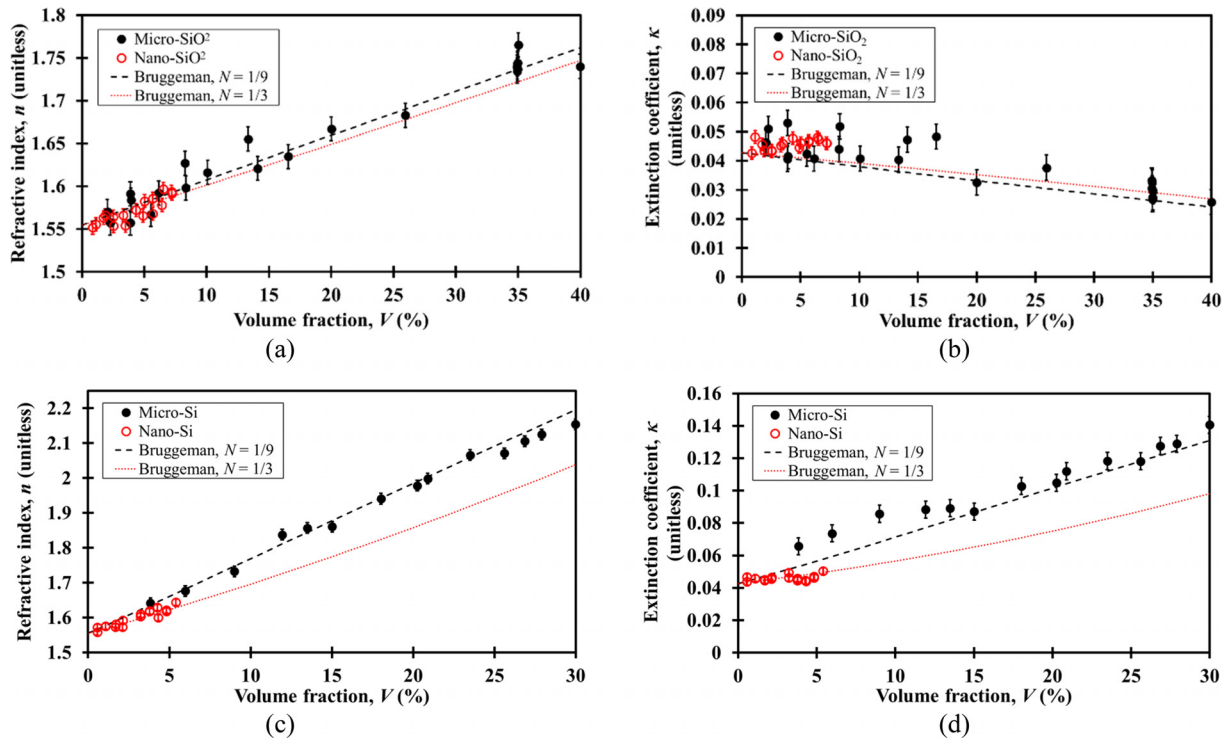

FIG. 3. Refraction and absorption characteristics of composites composed of SiO_2 and Si (roughly spherical) nanoparticles and (highly irregular) microparticles within a PDMS host. The experimental and theoretical results are shown for the (a) refractive index of the nano-SiO_2 and micro-SiO_2 composites, (b) extinction coefficient of the nano-SiO_2 and micro-SiO_2 composites, (c) refractive index of the nano-Si and micro-Si composites, and (d) extinction coefficient of the nano-Si and micro-Si composites. The experimental results for the nano-SiO_2 and nano-Si composites are denoted by open red circles; the experimental results for the micro-SiO_2 and micro-Si composites are denoted by solid black circles. The theoretical results from the Bruggeman model for the nano-SiO_2 and nano-Si composites are denoted by dotted red curves, for a depolarization factor of $N = 1/3$; the theoretical results from the Bruggeman model for the micro-SiO_2 and micro-Si composites are denoted by dashed black curves, for a depolarization factor of $N = 1/9$. The displayed error bars show the standard deviations in the measurements arising from inaccuracies in sample thickness and homogeneity.

The theory for the nano-SiO_2 composites is in contrast to this. It shows poor agreement, at a correlation coefficient of –0.50, with the experimental results, having a standard deviation of 2.1×10^{-3}, if the above extinction coefficient of 2.8×10^{-4} is applied. This disagreement is because the absorption in the SiO_2 nanoparticles is greater than that of the SiO_2 microparticles. We attribute this to the especially high surface-to-volume ratio of the SiO_2 nanoparticles, which forms a dense manifold of surface states[17] and exhibits absorption well beyond that of the SiO_2 microparticles and bulk.

Figure 3(c) shows theoretical and experimental results for the refractive index of the nano-Si and micro-Si composites. The experimental results show an increasing refractive index for the nano-Si composites, from 1.56 to 1.65 as the volumetric fraction rises to 5%, and an increasing refractive index for the micro-Si composites, from 1.56 to 2.2 as the volumetric fraction rises to 30%, which suggests that the refractive index of the Si is greater than that of PDMS. The theoretical results of the generalized Bruggeman model are obtained by curve-fitting Eq. (1) with the refractive index of Si extracted as a fitting parameter and the depolarization factors of the nanoparticles and microparticles fixed at the aforementioned values of $N = 1/3$ and $N = 1/9$, respectively. Overall, the results for the nano-Si and micro-Si composites show good agreement between the experiment, with respective standard deviations of 8.7×10^{-3} and 1.5×10^{-2}, and theory, at respective correlation coefficients of +0.93 and +0.99. Moreover, the fitting yields a refractive index of 3.42 for the Si, which agrees with the literature.[4] The differing depolarization factors applied here for the Si nanoparticles and microparticles arise from similar reasons to those given for the SiO_2 nanoparticles and microparticles. Specifically, the Si nanoparticles have a roughly spherical shape, which gives the depolarization factor of $N = 1/3$, while the Si microparticles have a highly irregular shape, which reduces the depolarization factor to $N = 1/9$. Ultimately, it is seen that the differing depolarization factors of the nanoparticles and microparticles yield a significant difference in Fig. 3(c). The dotted red curve for the nano-Si composites is well below the dashed black curve for the micro-Si composites. This suggests that depolarization is a noteworthy consideration in composites having a high index contrast between the inclusions and host—as is the case for these Si nanoparticles and microparticles in PDMS.

Figure 3(d) shows theoretical and experimental results for the extinction coefficient of the nano-Si and micro-Si composites. The experimental results show an increasing extinction coefficient for both the nano-Si composites, from 0.044 to 0.052 as the volumetric fraction rises to 5%, and the micro-Si composites, from 0.044 to 0.13 as the volumetric fraction rises to 30%. These similar trends suggest that the

extinction coefficient of the Si is greater than that of PDMS. The theoretical results of the Bruggeman model are obtained by curve-fitting Eq. (1) with the extinction coefficient of Si extracted as a fitting parameter and the depolarization factors of the nanoparticles and microparticles fixed at the aforementioned values of $N = 1/3$ and $N = 1/9$, respectively. The results for the micro-Si composites show good agreement between the experiment, with a standard deviation of 5.3×10^{-3}, and theory, at a correlation coefficient of +0.98. However, such fitting yields an extinction coefficient of 0.32 for the Si, which is far higher than the literature value of 2×10^{-4} seen for high-resistivity Si.[4] This discrepancy can be attributed to free-carrier dispersion and fit to the Drude model, assuming that the plasmon frequency due to confinement in the microparticles is well below the applied frequency range.[18] For the micro-Si composites, fitting the Drude model at a plasma frequency of 2.3 THz and a scatter time of 50 fs gives good agreement with the measured data. The results for the nano-Si composites show weak agreement between the experiment, with a standard deviation of 2.1×10^{-3}, and theory, at a correlation coefficient of +0.36. We attribute the weak correlation seen here not to free-carrier dispersion but instead to the high surface-to-volume ratio of the Si nanoparticles—like that seen for the nano-SiO_2 composites in Fig. 3(b). Again, the high surface-to-volume ratio of the Si nanoparticles forms a dense manifold of surface states,[17] which leads to absorption beyond that of the Si microparticles and bulk.

In light of the above findings, it can be concluded that the inclusion morphology and index contrast should be considered together in the refraction and absorption characteristics of composites within the THz spectrum. This is true even when the composites are formed from deeply subwavelength inclusions. The refraction characteristics showed a heightened dependence on the inclusions' shape when their index contrast with respect to the host became sufficiently large. This dependence manifested itself through differing trends for the refractive index of the nano-Si composite (with roughly spherical inclusions) and micro-Si composite (with highly irregular inclusions). Such trends could only be suitably characterized by the generalized Bruggeman model by introducing its shape-dependent depolarization factor—given the significant terahertz field depolarization that occurs within inclusions at high index contrasts and the dependence of the depolarization fields on the inclusions' shape. The absorption characteristics showed a heightened dependence on the inclusions' size when the size became sufficiently small. This dependence manifested itself through differing trends for the extinction coefficient of the nano-SiO_2 composite and micro-SiO_2 composite. The differences came about from the increased surface-to-volume ratio and surface state density of the SiO_2 nanoparticles, which raised their absorption beyond that of the SiO_2 microparticles and the bulk. Ultimately, such findings can lay the groundwork for future studies and applications of composites within the THz spectrum.

This work was supported in part by the Natural Sciences and Engineering Research Council of Canada (NSERC RGPIN-2017-04073), the Canadian Foundation for Innovation (CFI LOF 16659), and Western Economic Diversification Canada.

REFERENCES

[1]N. V. Chernomyrdin, A. O. Schadko, S. P. Lebedev, V. L. Tolstoguzov, V. N. Kurlov, I. V. Reshetov, I. E. Spektor, M. Skorobogatiy, S. O. Yurchenko, and K. I. Zaytsev, "Solid immersion terahertz imaging with sub-wavelength resolution," Appl. Phys. Lett. **110**, 221109 (2017).
[2]I. F. Akyildiz, J. M. Jornet, and C. Han, "Terahertz band: Next frontier for wireless communications," Phys. Commun. **12**, 16 (2014).
[3]B. Ung, A. Dupuis, K. Stoeffler, C. Dubois, and M. Skorobogatiy, "High-refractive-index composite materials for terahertz waveguides: Trade-off between index contrast and absorption loss," J. Opt. Soc. Am., B **28**, 917 (2011).
[4]D. Grischkowsky, S. Keiding, M. Van Exter, and C. Fattinger, "Far-infrared time-domain spectroscopy with terahertz beams of dielectrics and semiconductors," J. Opt. Soc. Am., B **7**, 2006 (1990).
[5]S. Alfihed, M. H. Bergen, J. F. Holzman, and I. G. Foulds, "A detailed investigation on the terahertz absorption characteristics of polydimethylsiloxane (PDMS)," Polym. J. **153**, 325 (2018).
[6]A. Podzorov and G. Gallot, "Density of states and vibrational modes of PDMS studied by terahertz time-domain spectroscopy," Chem. Phys. Lett. **495**, 46 (2010).
[7]S. Wietzke, C. Jansen, F. Rutz, D. M. Mittleman, and M. Koch, "Determination of additive content in polymeric compounds with terahertz time-domain spectroscopy," Polym. Test. **26**, 614 (2007).
[8]D. Headland, P. Thurgood, D. Stavrevski, W. Withayachumnankul, D. Abbott, M. Bhaskaran, and S. Sriram, "Doped polymer for low-loss dielectric material in the terahertz range," Opt. Mater. Express **5**, 1373 (2015).
[9]M. M. Nazarov, E. V. Khaydukov, A. G. Savelyev, V. I. Sokolov, A. S. Akhmanov, A. P. Shkurinov, and V. Y. Panchenko, "Terahertz response of a polymer composite with high concentration of silicon micro- and nanoparticles," Nanotechnol. Russia **10**, 247 (2015).
[10]X. Wang, Y. Li, B. Cai, and Y. Zhu, "High refractive index composite for broadband antireflection in terahertz frequency range," Appl. Phys. Lett. **106**, 231107 (2015).
[11]M. Scheller, S. Wietzke, C. Jansen, and M. Koch, "Modelling heterogeneous dielectric mixtures in the terahertz regime: A quasi-static effective medium theory," J. Phys. D **42**, 065415 (2009).
[12]M. Kaushik, B. W. Ng, B. M. Fischer, and D. Abbott, "Terahertz scattering by granular composite materials: An effective medium theory," Appl. Phys. Lett. **100**, 011107 (2012).
[13]J. Lloyd-Hughes and T. I. Jeon, "A review of the terahertz conductivity of bulk and nano-materials," J. Infrared, Millimeter, Terahertz Waves **33**, 871 (2012).
[14]D. Polder and J. H. Van Santeen, "The effective permeability of mixtures of solids," Physica **12**, 257 (1946).
[15]A. Sihvola, "Dielectric polarization and particle shape effects," J. Nanomater. **2007**, 45090 (2007).
[16]M. Z. Rong, M. Q. Zhang, and W. H. Ruan, "Surface modification of nanoscale fillers for improving properties of polymer nanocomposites: A review," J. Mater. Sci. Technol. **22**, 787 (2006).
[17]D. Bera, L. Qian, T. K. Tseng, and P. H. Holloway, "Quantum dots and their multimodal applications: A review," Materials **3**, 2260 (2010).
[18]H. K. Nienhuys and V. Sundström, "Influence of plasmons on terahertz conductivity measurements," Appl. Phys. Lett. **87**, 012101 (2005).